physica status solidi b
www.pss-b.com

Third-Order Susceptibility of Lithium Niobate: Influence of Polarons and Bipolarons

Agnieszka L. Kozub, Uwe Gerstmann, and Wolf Gero Schmidt*

The third-order susceptibility $\chi^{(3)}$ of lithium niobate ($LiNbO_3$) is calculated within a Berry-phase formulation of the dynamical polarization based on the electronic structure obtained within density-functional theory (DFT). Maximum $|\chi^{(3)}_{zzzz}|$ values of the order of 10^{-19} m^2 V^{-2} are calculated for photon energies between 1.2 and 2 eV, i.e., in the lower half of the optical bandgap of lithium niobate. Both free and bound electron (bi)polarons are found to lead to a remarkable enhancement of the third-order susceptibility for photon energies below 1 eV.

1. Introduction

Lithium niobate ($LiNbO_3$, LN) forms a ferroelectric crystal with a 10-atom unit cell, its crystal structure is shown in **Figure 1**. It is an important material for various linear and nonlinear optical applications. This is due to its unique physical properties, such as strong optical nonlinearity and large electro-optic, acousto-optic, and piezoelectric coefficients, as well as its wide transparency window and high refractive index.[1] Lithium niobate is a semiconductor, the optical bandgap of which has been measured at 3.78 eV.[2]

Generally, the polarization **P** of a medium may be expressed as a power series of the incident field $\mathbf{E}(\omega)$ of frequency ω.[3] In components, it is given by

$$\begin{aligned} P_\alpha(\omega) = &\sum_\beta \chi^{(1)}_{\alpha\beta}(\omega,\omega)E_\beta(\omega) \\ &+ \sum_{\beta\gamma} \chi^{(2)}_{\alpha\beta\gamma}(\omega,\omega_1,\omega_2)E_\beta(\omega_1)E_\gamma(\omega_2) \\ &+ \sum_{\beta\gamma\xi} \chi^{(3)}_{\alpha\beta\gamma\xi}(\omega,\omega_1,\omega_2,\omega_3)E_\beta(\omega_1)E_\gamma(\omega_2)E_\xi(\omega_3) \\ &+ \cdots \end{aligned} \tag{1}$$

where α, β, γ, and ξ stand for the Cartesian coordinates and $\chi^{(n)}(\omega)$ is the nth-order frequency-dependent susceptibility, a $(n+1)$-rank tensor.

In the case of LN, much work has been dedicated to measure and calculate the linear and second-order susceptibilities $\chi^{(1)}$ and $\chi^{(2)}$.[4–6] Far less is known about the third-order susceptibility $\chi^{(3)}(\omega) := \chi^{(3)}(3\omega,\omega,\omega,\omega)$, relevant to the process of third-harmonic generation (THG). Moreover, the existing measurements arrive at vastly different values. The frequently cited value $|\chi^{(3)}| = 2.4 \times 10^{-13}$ m^2 V^{-2} measured at a wavelength of $\lambda = 514$ nm by Henari et al.[7] is five orders of magnitude larger than the value for Si,[3] known as a material with relatively large third-order susceptibility. Choubey et al.[8] determined a THG coefficient that is several orders of magnitude smaller: At a wavelength of $\lambda = 1064$ nm, they obtained $|\chi^{(3)}| = 3.9 \times 10^{-18}$ m^2 V^{-2}. The data obtained by Li et al.[9] and Wang and coworkers[10] are another two orders of magnitude smaller than the latter value. They determined $|\chi^{(3)}| = 1.04 \times 10^{-20}$ m^2 V^{-2} and $|\chi^{(3)}| = 1.5 \times 10^{-20}$ m^2 V^{-2}, respectively, at a wavelength of $\lambda = 532$ nm.

These striking differences in the THG coefficients measured for one of the most frequently used nonlinear optical materials motivate the present study, where density-functional theory (DFT) based calculations are employed to determine $\chi^{(3)}$ from first principles. All nonzero, distinguishable tensor elements of stoichiometric LN are calculated. Additionally, it is explored to what extent the THG in LN is affected by polaron formation. Electron polarons in lithium niobate are generated optically within a few hundred femtoseconds[11,12] and form preferentially at specific trapping sites, which may be locally modified by doping.[13] Recently, it has been shown that the second-harmonic generation (SHG) in LN is strongly enhanced by electron polarons.[14]

2. Results

The methodology described in Section 4 has been used to calculate $\chi^{(3)}(\omega)$ tensor elements for stoichiometric LN in its ideal bulk configuration, see **Figure 2**. Clearly, from all considered tensor elements, the intensity of $|\chi^{(3)}_{zzzz}(\omega)|$ is highest in the considered energy range. An onset of $|\chi^{(3)}(\omega)|$ for photon energies larger than 1 eV is calculated for the ideal bulk, followed by a peak at about 1.3 eV for the case of $|\chi^{(3)}_{zzzz}(\omega)|$ and 1.4 eV for other coefficients. Thus, for photon energies corresponding to

A. L. Kozub, U. Gerstmann, W. G. Schmidt
Department Physik
Universität Paderborn
33095 Paderborn, Germany
E-mail: agnieszka.kozub@uni-paderborn.de

The ORCID identification number(s) for the author(s) of this article can be found under https://doi.org/10.1002/pssb.202200453.

DOI: 10.1002/pssb.202200453

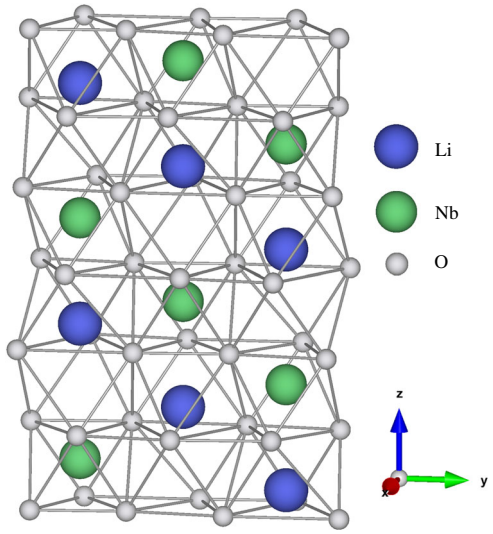

Figure 1. Crystal structure of stoichiometric lithium niobate. Blue, green, and gray balls represent lithium, niobium, and oxygen atoms, respectively.

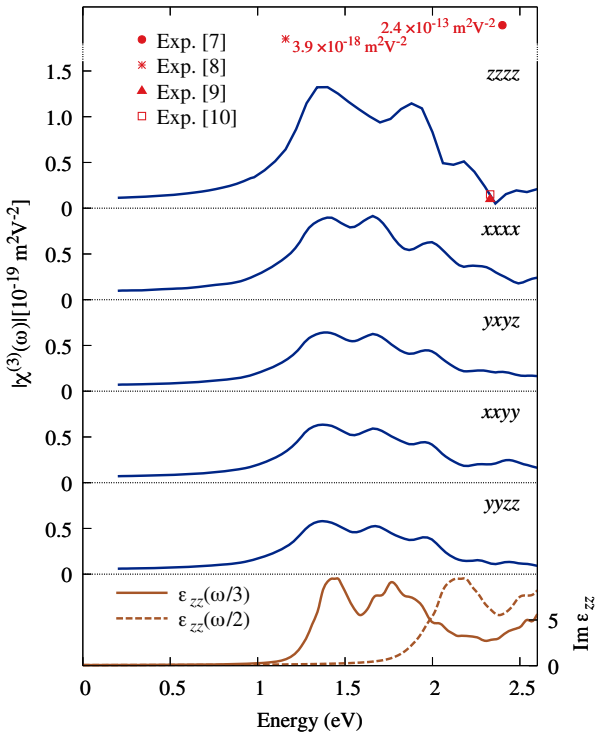

Figure 2. Calculated nonzero tensor elements of $|\chi^{(3)}(\omega)|$ for stoichiometric $LiNbO_3$. Experimental data for $|\chi^{(3)}|$[7–10] are indicated. Note that the data from Refs. [7,8] do not fit to the scale. Energy-scaled calculations for the imaginary part of the LN dielectric function are shown in the bottom panel for comparison.

approximately one-third of the LN optical gap, the maximum value of $|\chi^{(3)}(\omega)|$ is assumed. The $|\chi^{(3)}_{zzzz}(\omega)|$ maximum value is slightly larger than $10^{-19}\,m^2\,V^{-2}$ and thus considerably smaller than the data measured in Refs. [7,8]. In contrast, the calculated data agree very well with the third-order susceptibilities measured in Refs. [9,10] at photon energies of 2.33 eV, corresponding to a wavelength of 532 nm, as shown in Figure 2.

The bottom graph of Figure 2 shows for comparison calculations of the LN linear optical response, i.e., the imaginary part of the dielectric function, energy-scaled to one-third and one-half frequencies. The comparison suggests that the main peak of the THG response results from three-photon processes, while the less pronounced second and third feature has contributions from two-photon processes and one-photon resonances, respectively. This interpretation agrees with very recent findings by Sanna and coworkers.[6]

Electron polarons and bipolarons give rise to polaronic states inside the LN bandgap.[15,16] The population of these levels, for example, by illumination, leads to strongly enhanced $\chi^{(2)}$ coefficients and thus allows for the spatial and transient modification of the SHG in macroscopic samples.[14] Do these polaronic states also affect the THG in lithium niobate?

To answer this question, we focus on the polaron structures recently established in Ref. [17], see **Figure 3**: Free polarons (F) correspond to excess electrons localized at regular Nb_{Nb} ions, $F(Nb_{Nb})$. Bound polarons (P) form either at Nb_{Li} point defects, $P(Nb_{Li})$, or at Nb_V–V_{Li} defect pairs, $P(Nb_V–V_{Li})$. Bipolarons (B) correspond to two excess electrons, one of them bound to a defect-related Nb. Here we consider $B(Nb_{Li})$ and $B(Nb_V–V_{Li})$. Free and bound polarons may occur in axially symmetric and tilted, i.e., Jahn–Teller distorted configurations. In the axially symmetric configuration, the Nb atoms carrying the excess electrons relax along the [001] direction, which results in orbitals of d_{z^2} type. In the tilted configurations, the Nb atoms relax perpendicular to the [001] direction. This results in a clover-like shape of orbitals of the d_{yz} character, see Figure 3.

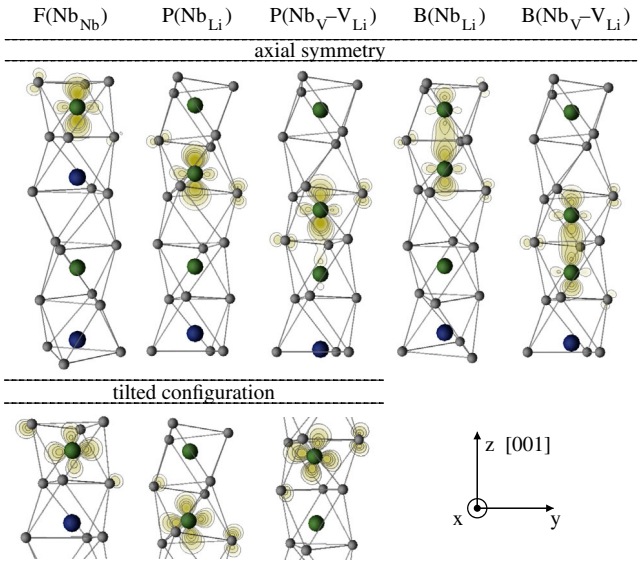

Figure 3. Polaron structures considered in this work, together with the corresponding charge densities. Free polarons (F), bound polarons (P), and bipolarons (B) are shown in the axial symmetric configurations; for F and P polarons, the tilted configurations are also shown. The color scheme corresponds to Figure 1.

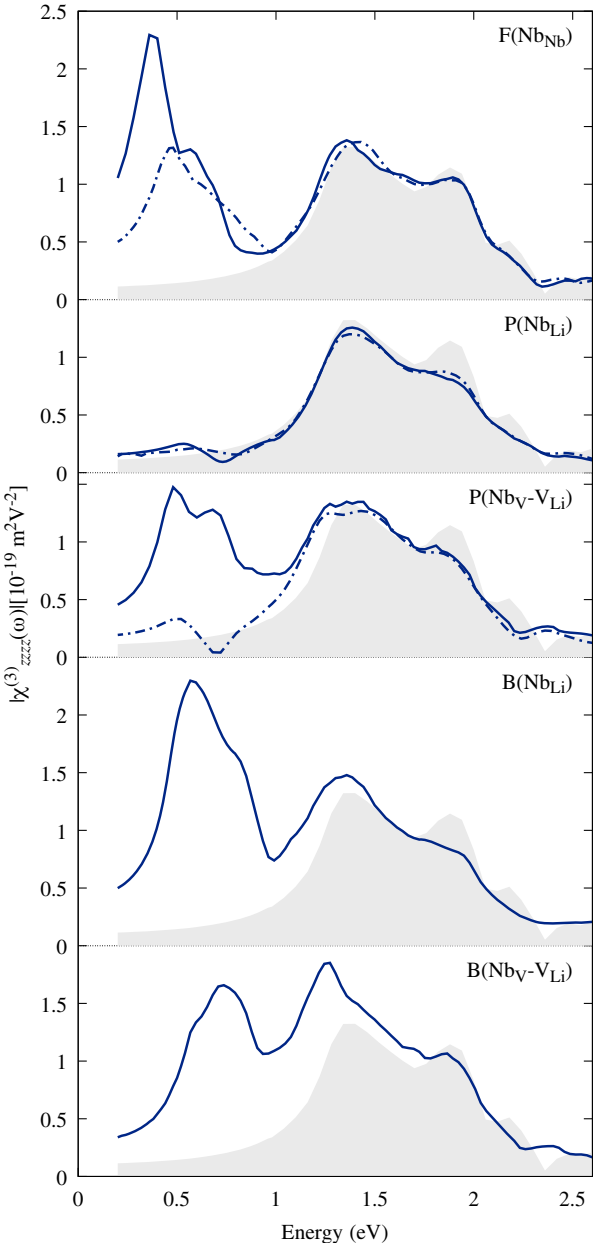

Figure 4. Calculated $|\chi^{(3)}_{zzzz}(\omega)|$ for supercells containing polarons. Solid lines correspond to structures with axial symmetry, dashed lines to tilted configurations. Shaded area corresponds to the result for stoichiometric $LiNbO_3$.

As shown in **Figure 4**, polaron formation leads to a giant enhancement of $|\chi^{(3)}_{zzzz}(\omega)|$ for low photon energies. This holds for free polarons and bipolarons, in particular B(Nb$_{Li}$). Here strong peaks at photon energies of about 0.4 and 0.6 eV are predicted. It is interesting to note that free polarons strongly enhance the THG, while they were found to be of minor influence on the SHG.[14] This can be understood, however, by means of symmetry: Free polarons formed at regular Nb_{Nb} ions largely obey inversion symmetry,[17] thus their SHG response is suppressed. The influence of bound polarons on the THG is

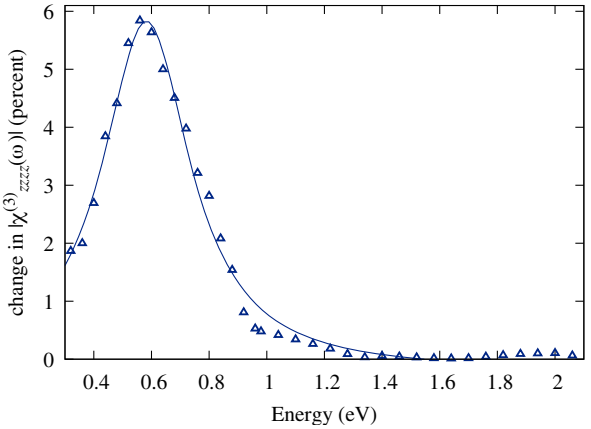

Figure 5. Calculated relative change in $|\chi^{(3)}_{zzzz}(\omega)|$ due to bipolaron B(Nb$_{Li}$) formation in bulk $LiNbO_3$, assuming a polaron density of 4.4×10^{24} m^{-3} as measured in Ref. [11]. The smooth line is to guide the eye.

relatively minor. A pronounced signal is calculated only for P(Nb$_V$–V$_{Li}$) with axial symmetry. Above 1 eV, the calculated $|\chi^{(3)}_{zzzz}(\omega)|$ for all polarons is very similar and mimics that of stoichiometric LN.

The data shown in Figure 4 cannot directly be compared with the experiment. On the one hand, the present calculations are performed within the independent-particle approximation (IPA). Optical excitations are known, however, to be influenced by electronic many-body effects. Self-energy effects will blueshift the excitation energies and decrease the susceptibilities. Both effects are partially compensated by excitonic effects.[18,19] Therefore, we expect the IPA calculations to be at least qualitatively correct. On the other hand, the present polaron calculations have been performed using 80-atom cells. This corresponds to a polaron density far higher than typically observed experimentally. The steady-state density of bipolarons at room temperature in congruent LN without illumination has been reported to be about 6.7×10^{23} m^{-3}.[20] Optical excitation may increase this value considerably.[11,12] Buse and co-workers report polaron densities of 4.4×10^{24} m^{-3}.[11] This value may be used to rescale the polaron-induced changes of $|\chi^{(3)}_{zzzz}(\omega)|$ calculated for the 80-atom cell to experimentally accessible polaron densities. The according order-of-magnitude estimate for the polaron-induced change of $|\chi^{(3)}_{zzzz}(\omega)|$ compared the ideal bulk is shown in **Figure 5**. A maximum change of up to 6% is calculated for B(Nb$_{Li}$) formation. This is the same order of magnitude as the relative change in SHG due to the bipolaron formation in LN.[14] It suggests that also in real samples the polaronic enhancement of the THG efficiency calculated here will be observable.

3. Conclusion

In summary, THG in lithium niobate has been calculated from first principles. For stoichiometric crystals, $|\chi^{(3)}_{zzzz}|$ values larger than 10^{-19} m^2 V^{-2} are calculated, in good agreement with some experimental data. The present calculations do not support, however, earlier claims that LN has a third-order susceptibility that is

several orders of magnitude larger than measured for silicon. According to the present calculations, the THG in LN may be substantially enhanced by polarons. The polaron distribution in the crystal can be modified spatially by doping and is strongly increased by optical excitation. The polaronic enhancement of the nonlinear optical coefficients predicted here thus suggests a way to control LN THG in space and time.

4. Methodology

Methodologically, the approach used in Ref. [14] was largely followed. In detail, the Quantum Espresso[21,22] implementation of DFT was used to perform electronic-structure calculations. The PBEsol functional[23] was used to describe the electron exchange and correlation effects within the generalized gradient approximation. The DFT+U scheme[24] was used to account for the strong localization of the Nb 4d electrons. The Hubbard U was chosen large enough to enable the electron self-trapping characteristic for polaron formation, see discussion in Ref. [15]. Here, self-consistently determined U values were used, i.e., 4.7 eV for the regular Nb atoms and for those carrying free polarons; 5.2 eV for Nb_{Li} antisite and Nb_v interstitial atoms. Spin-polarized calculations were performed to account for unpaired electrons. Stoichiometric LN was modeled within a 10-atom unit cell. Here a $6 \times 6 \times 6$ Γ-centered $\mathbf{k}$-point mesh was used for Brillouin sampling. The nonlinear susceptibilities were calculated using 70 electronic bands – 32 occupied and 38 empty states. The polaron structures were modeled within 80-atom supercells. In this case, a $3 \times 3 \times 3$ Γ-centered $\mathbf{k}$-point mesh and 500 electronic bands were used. This included 256 occupied states and one defect band for free polarons, 260 occupied states and one defect band for bound polarons, and 263 occupied states and one defect band for bipolarons.

The nonlinear susceptibilities were obtained from the real-time evolution of the Bloch electrons in a uniform time-dependent electric field following the Berry-phase approach proposed by Attaccalite and Grüning.[25] This approach was successfully used for SHG calculations for various semiconductors. In this method, the time-dependent polarization is computed from the evolution of valence states $|v_{n\mathbf{k}}\rangle$, described by the equations of motion

$$i\hbar \frac{\partial}{\partial t} |v_{n\mathbf{k}}\rangle = (H^{\mathrm{KS}}_{\mathbf{k}} + i\mathbf{E} \cdot \tilde{\partial}_{\mathbf{k}}) |v_{n\mathbf{k}}\rangle \tag{2}$$

where $H^{\mathrm{KS}}_{\mathbf{k}}$ corresponds to the Kohn–Sham Hamiltonian. The term $\mathbf{E} \cdot \tilde{\partial}_{\mathbf{k}}$ in Equation (2) describes the coupling to the external electric field $\mathbf{E}$. Finally, $\chi^{(3)}(\omega)$ is derived from the power series expansion of the calculated polarization. The technical parameters are chosen as in Ref. [14], apart from the simulation and the dephasing times. These times have been increased to 70 and 50 fs, respectively, for better convergence.

The linear optical response of stoichiometric LN was calculated for comparison. The respective calculations are performed within the independent particle approximation using the Yambo package.[26,27] Here 32 occupied and 168 empty bands of a 10-atom LN cell were employed in conjunction with a $6 \times 6 \times 6$ sampling of the Brillouin zone.

Acknowledgements

Deutsche Forschungsgemeinschaft (DFG) TRR 142/3-2022, project number 231447078 is acknowledged for financial support. The authors thank the Paderborn Center for Parallel Computing (PC^2) and the Höchstleistungs–Rechenzentrum Stuttgart (HLRS) for grants of high-performance computer time.

Open Access funding enabled and organized by Projekt DEAL.

Conflict of Interest

The authors declare no conflict of interest.

Data Availability Statement

The data that support the findings of this study are available from the corresponding author upon reasonable request.

Keywords

density-functional theory, lithium niobate, polarons, third-harmonic generation

Received: September 22, 2022
Revised: November 16, 2022
Published online: December 2, 2022

[1] R. S. Weis, T. K. Gaylord, *Appl. Phys. A* **1985**, *37*, 191.
[2] A. Dhar, A. Mansingh, *J. Appl. Phys.* **1990**, *68*, 5804.
[3] R. W. Boyd, *Nonlinear Optics*, Academic Press, London **2020**.
[4] I. Shoji, T. Kondo, A. Kitamoto, M. Shirane, R. Ito, *J. Opt. Soc. Am. B* **1997**, *14*, 2268.
[5] A. Riefer, S. Sanna, A. Schindlmayr, W. G. Schmidt, *Phys. Rev. B* **2013**, *87*, 195208.
[6] C. Dues, M. J. Müller, S. Chatterjee, C. Attaccalite, S. Sanna, *Phys. Rev. Mater.* **2022**, *6*, 065202.
[7] F. Z. Henari, K. Cazzini, F. El Akkari, W. J. Blau, *J. Appl. Phys.* **1995**, *78*, 1373.
[8] R. Choubey, R. Trivedi, M. Das, P. Sen, P. Sen, S. Kar, K. Bartwal, R. Ganeev, *J. Cryst. Growth* **2009**, *311*, 2597.
[9] H. Li, F. Zhou, X. Zhang, W. Ji, *Appl. Phys. B* **1997**, *64*, 659.
[10] Y. Wang, Y. Niu, G. Wang, Y. Sun, C. Liu, *J. Alloys Compd.* **2019**, *778*, 691.
[11] O. Beyer, D. Maxein, T. Woike, K. Buse, *Appl. Phys. B* **2006**, *83*, 527.
[12] H. Badorreck, S. Nolte, F. Freytag, P. Baune, V. Dieckmann, M. Imlau, *Opt. Mater. Express* **2015**, *5*, 2729.
[13] O. F. Schirmer, M. Imlau, C. Merschjann, B. Schoke, *J. Phys.: Condens. Matter* **2009**, *21*, 123201.
[14] A. L. Kozub, A. Schindlmayr, U. Gerstmann, W. G. Schmidt, *Phys. Rev. B* **2021**, *104*, 174110.
[15] M. Krenz, U. Gerstmann, W. G. Schmidt, *Appl. Phys. A* **2022**, *128*, 480.
[16] F. Schmidt, A. L. Kozub, U. Gerstmann, W. G. Schmidt, A. Schindlmayr, *Crystals* **2021**, *11*, 542.
[17] F. Schmidt, A. L. Kozub, T. Biktagirov, C. Eigner, C. Silberhorn, A. Schindlmayr, W. G. Schmidt, U. Gerstmann, *Phys. Rev. Res.* **2020**, *2*, 043002.
[18] R. Leitsmann, W. G. Schmidt, P. H. Hahn, F. Bechstedt, *Phys. Rev. B* **2005**, *71*, 195209.

[19] A. Riefer, W. G. Schmidt, *Phys. Rev. B* **2017**, *96*, 235206.
[20] C. Merschjann, B. Schoke, D. Conradi, M. Imlau, G. Corradi, K. Polgár, *J. Phys.: Condens. Matter* **2008**, *21*, 015906.
[21] P. Giannozzi, S. Baroni, N. Bonini, M. Calandra, R. Car, C. Cavazzoni, D. Ceresoli, G. L. Chiarotti, M. Cococcioni, I. Dabo, A. D. Corso, S. de Gironcoli, S. Fabris, G. Fratesi, R. Gebauer, U. Gerstmann, C. Gougoussis, A. Kokalj, M. Lazzeri, L. Martin-Samos, N. Marzari, F. Mauri, R. Mazzarello, S. Paolini, A. Pasquarello, L. Paulatto, C. Sbraccia, S. Scandolo, G. Sclauzero, A. P. Seitsonen, et al., *J. Phys.: Condens. Matter* **2009**, *21*, 395502.
[22] P. Giannozzi, O. Andreussi, T. Brumme, O. Bunau, M. B. Nardelli, M. Calandra, R. Car, C. Cavazzoni, D. Ceresoli, M. Cococcioni, N. Colonna, I. Carnimeo, A. D. Corso, S. de Gironcoli, P. Delugas, R. A. DiStasio, A. Ferretti, A. Floris, G. Fratesi, G. Fugallo, R. Gebauer, U. Gerstmann, F. Giustino, T. Gorni, J. Jia, M. Kawamura, H.-Y. Ko, A. Kokalj, E. Küçükbenli, M. Lazzeri, et al., *J. Phys.: Condens. Matter* **2017**, *29*, 465901.
[23] M. Friedrich, A. Riefer, S. Sanna, W. G. Schmidt, A. Schindlmayr, *J. Phys.: Condens. Matter* **2015**, *27*, 385402.
[24] M. Cococcioni, S. de Gironcoli, *Phys. Rev. B* **2005**, *71*, 035105.
[25] C. Attaccalite, M. Grüning, *Phys. Rev. B* **2013**, *88*, 235113.
[26] A. Marini, C. Hogan, M. Grüning, D. Varsano, *Comput. Phys. Commun.* **2009**, *180*, 1392.
[27] D. Sangalli, A. Ferretti, H. Miranda, C. Attaccalite, I. Marri, E. Cannuccia, P. Melo, M. Marsili, F. Paleari, A. Marrazzo, G. Prandini, P. Bonfa, M. O. Atambo, F. Affnito, M. Palummo, A. Molina-Sánchez, C. Hogan, M. Grüning, D. Varsano, A. Marini, *J. Phys.: Condens. Matter* **2019**, *31*, 325902.